JOURNAL OF COMPUTATIONAL PHYSICS 10, 379–399 (1972)

On a Finite-Difference Approach to Turbulence Problems

F. M. GALLOWAY* AND R. J. ADLER

Case Western Reserve University

Received January 11, 1972

Using a new, energy conserving finite-difference scheme for the unaveraged Navier–Stokes equations, pressure driven flow in a square duct is calculated for meshes of 7, 9, 11 and 17 points in each of three space directions. Both fully developed laminar and turbulent solutions are obtained as a function of the pressure drop imposed. The solutions are independent of initial conditions. Friction factor–Reynolds number relations, mean velocity profiles, Reynolds stress profiles and mean turbulence energy profiles qualitatively resemble data from physical flows. Improvement is noted as the mesh is refined. However, quantitative results would require an excessively fine mesh with impractically large computing requirements.

1. INTRODUCTION

Three-dimensional incompressible turbulent flow in a square duct is calculated numerically. A mean axial pressure gradient drives the flow. The flow is computed in time from an initial state to a statistically stationary state. The computations are made with a new energy conserving finite difference approximation to the unaveraged Navier–Stokes equations. No closure theories are used.

The computations were performed, first, to test a new energy conserving scheme discovered by the authors, and second, to determine the computing effort required for this direct approach. Based on previous work, particularly for homogeneous turbulence calculations [1] and shear flow turbulence calculations using turbulence theories [2], the computing effort is known to be large for high Reynolds numbers. However, no systematic experimental determination of computing effort has been made for three-dimensional shear flow turbulence calculated by finite-differencing of the unaveraged Navier–Stokes equations. (See [3] for an a priori estimate.)

* F. M. Galloway is currently with Cleveland State University.

2. Physical and Mathematical Description

The square duct and dimensionless coordinate system are described in Fig. 1.

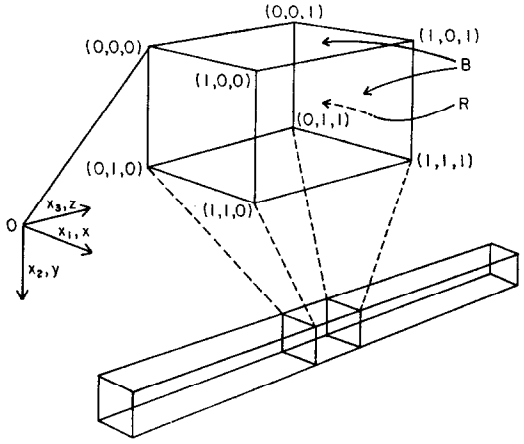

FIG. 1. The dimensionless coordinate system.

It is assumed that the fluid motion within the region R, for an incompressible Newtonian fluid, is governed by the dimensionless Navier–Stokes equation

$$\frac{\partial U_i}{\partial t} + U_j \frac{\partial U_i}{\partial x_j} = -\frac{\partial P}{\partial x_i} - \delta_{i3} \frac{\partial \bar{P}}{\partial x_3} + \frac{1}{\mathrm{Re}} \frac{\partial^2 U_i}{\partial x_j \partial x_j} \tag{1}$$

and by the continuity equation

$$\partial U_i / \partial x_i = 0, \tag{2}$$

where $i, j = 1, 2, 3$ unless otherwise noted, Re is the Reynolds number ($\mathrm{Re} \equiv D\bar{U}_3 \rho/\mu$), δ_{ij} is the Kronecker delta, "3" is the axial direction, $\partial \bar{P}/\partial x_3$ represents the mean axial pressure gradient, the bar represents ensemble average, and P is the deviation of the pressure from the assigned mean pressure gradient. Equations (1) and (2) may be put in a form more convenient for finite-difference solution by taking the divergence of (1) and simplifying the result with (2). Thus, instead of (2), the fourth independent relation becomes

$$\partial^2 P / \partial x_i \partial x_i = -(\partial/\partial x_i)[U_j(\partial U_i/\partial x_j)]. \tag{3}$$

Note also that (1) may be written in the slightly different form;

$$\frac{\partial U_i}{\partial t} + \frac{\partial (U_i U_j)}{\partial x_j} = -\frac{\partial P}{\partial x_i} - \delta_{i3} \frac{\partial \bar{P}}{\partial x_i} + \frac{1}{\mathrm{Re}} \frac{\partial^2 U_i}{\partial x_j \partial x_j} \tag{4}$$

again by making use of (2) to put the convective terms in the altered form. In this case, (3) takes the form

$$\partial^2 P/\partial x_i \partial x_i = -(\partial/\partial x_i)[\partial(U_i U_j)/\partial x_j]. \tag{5}$$

It will be found convenient to refer to both forms (1) and (4) when describing the finite-difference approximations in Section 3.

The boundaries of the test section indicated in Fig. 1 are treated as follows: Let B_W denote the part of B that is composed of the duct walls, B_a the entrance plane ($z = 0$) and B_b the exit plane ($z = 1$). Then the boundary conditions for the periodic test section are

On B_W

$$U_i = 0, i = 1, 2, 3, \tag{6}$$

$$\frac{\partial P}{\partial x_i} = \frac{1}{\mathrm{Re}} \frac{\partial^2 U_i}{\partial x_j \partial x_j}, \qquad i = 1, 2 \quad \text{and} \quad j = 1, 2, 3, \tag{7}$$

where i in (7) denotes the perpendicular direction to the section of B_W in question.

On B_a and B_b

$$U_i(x, y, 0) = U_i(x, y, 1), \qquad i = 1, 2, 3, \tag{8}$$

$$P(x, y, 0) = P(x, y, 1). \tag{9}$$

Equation (6) is the no slip condition for the velocity. Equation (7) is the compatible condition for the pressure, obtained by setting $U_i = 0$ in (1) or (4). Equation (8) represents a periodic condition imposed on the velocity in the axial direction. Thus the duct is considered to be made up of an infinite number of sequential adjacent sections, each identical to the region R in Fig. 1. This periodic condition on the velocity implies a periodic solution for the pressure deviation P also, since the differential Eq. (3) and the boundary conditions at the wall for the pressure deviation are identical in each of the sections if the velocity is periodic. Thus, condition (9) is obtained. A suitable criterion for choosing the length appears to be that the section is long enough such that entrance and exit conditions are essentially uncoupled, so that no significant changes in the answers would be obtained by using a longer test section. Turbulence correlation measurements in a channel [3] indicate that the largest "eddies" are about one-half the channel width, so that a length equal to the duct width, i.e., a cubic test section, should be sufficient. This assumption was checked by repeating one computation with a test section having a length twice the width. The resulting properties of the sustained state (see Table I) were essentially the same for both examples. Thus, a cubic

section was considered to be sufficient, and the results described in Section 4 were computed from such a section.

To complete the problem statement, an initial velocity field must be assigned. There is considerable freedom in this assignment, the only theoretical restriction being that the velocity must satisfy the continuity Eq. (2) and boundary conditions. In fact, for the numerical solution of the problem, several different initial conditions were tried and the sustained state was found to be independent of the particular initial conditions used.

Equations (1) and (3) (or several other combinations of Eqs. (1)–(5)), along with the boundary conditions (6)–(9) and appropriate initial conditions form an initial-boundary value problem for the dependent variables of pressure and velocity.

3. The Finite-Difference Approximations

The periodic test section and grid indices are shown in Fig. 2. The mesh spacing is constant and equal in each space direction and is denoted by h. The time increment (which is not necessarily constant during each computation) is denoted by Δt. Variables obtained at space-time mesh points from the finite-difference computation are denoted as, e.g., U^n_{ijk} as an approximation to the variable $U(x_i, y_j, z_k, t_n) = U\{(i-1)h, (j-1)h, (k-1)h, n\Delta t\}$ from the continuous problem. In order to treat some of the boundary conditions, it is convenient to define some variables at points one mesh interval outside the boundary. These points are denoted by, e.g., $i = 0$ which corresponds to $x_0 = -h$, $i = N + 1$

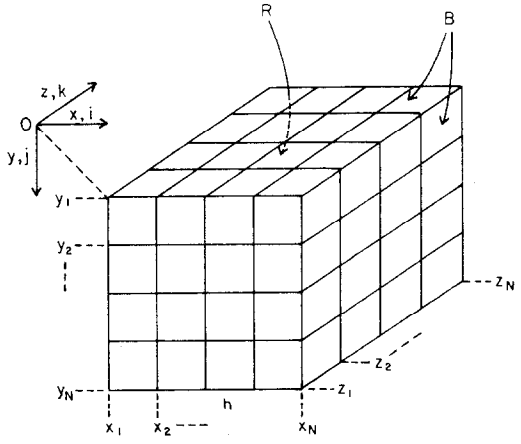

Fig. 2. Coordinate system and grid indices.

corresponding to $x_{N+1} = (N+1)h$, $j = 0$, corresponding to $y_0 = -h$, etc. The cartesian tensor notation of Section 2 is replaced by standard cartesian coordinate notation, i.e., x, y, z and U, V, W notation.

The finite-difference approximation used for the Navier–Stokes Eq. (1) is

$$\overbrace{\frac{U_{ijk}^{n+1} - U_{ijk}^{n-1}}{2\Delta t}}^{A} + \overbrace{\frac{1}{2}\left[\frac{(U_{i+1jk}^{n})^2 - (U_{i-1jk}^{n})^2}{2h} + \frac{U_{ij+1k}^{n}V_{ij+1k}^{n} - U_{ij-1k}^{n}V_{ij-1k}^{n}}{2h}\right.}^{B}$$

$$\overbrace{\left. + \frac{U_{ijk+1}^{n}W_{ijk+1}^{n} - U_{ijk-1}^{n}W_{ijk-1}^{n}}{2h} + U_{ijk}\left(\frac{U_{i+1jk}^{n} - U_{i-1jk}^{n}}{2h}\right)\right.}$$

$$\left. + V_{ijk}\left(\frac{U_{ij+1k}^{n} - U_{ij-1k}^{n}}{2h}\right) + W_{ijk}^{n}\left(\frac{U_{ijk+1}^{n} - U_{ijk-1}^{n}}{2h}\right)\right]$$

$$= \overbrace{-\frac{P_{i+1jk}^{n} - P_{i-1jk}^{n}}{2h}}^{C}$$

$$\overbrace{+\frac{1}{\mathrm{Re}}\left[\frac{U_{i+1jk}^{n} + U_{i-1jk}^{n} + U_{ij+1k}^{n} + U_{ij-1k}^{n} + U_{ijk+1}^{n} + U_{ijk-1}^{n} - 3(U_{ijk}^{n+1} + U_{ijk}^{n-1})}{h^2}\right]}^{D} \tag{10}$$

and similar equations for V and W. The approximation for the continuity Eq. (2) is

$$\frac{U_{i+1jk}^{n} - U_{i-1jk}^{n}}{2h} + \frac{V_{ij+1k}^{n} - V_{ij-1k}^{n}}{2h} + \frac{W_{ijk+1}^{n} - W_{ijk-1}^{n}}{2h} = 0. \tag{11}$$

The finite-difference version of the continuous elliptic equation for the pressure (3) is derived in a manner analagous with the derivation of the continuous equation. U_{ijk}^{n+1} is explicitly solved for from Eq. (10) and V_{ijk}^{n+1} and W_{ijk}^{n+1} are solved for from the similar equations for V and W. These expressions are substituted into Eq. (11) written at time $n+1$ so that the velocity at time $n+1$ is eliminated. The resulting equation is an elliptic difference equation for the pressure at time n in terms of (known) velocities at time n and $n-1$. The pressure field determined by this equation, when put into Eq. (10) and the similar equations for V and W, insures that the velocity field computed at time $n+1$ will satisfy the finite-difference version of the continuity equation (11). A detailed presentation of this development is available [4].

The boundary conditions of Section 2 are approximated as follows: Conditions (6) become

$$U^n_{1jk} = U^n_{i1k} = U^n_{Nik} = U^n_{iNk} = V^n_{1jk} = \cdots = W^n_{iNk} = 0. \tag{12}$$

Conditions (7) become

$$P^n_{2jk} - P^n_{0jk} = (4/Reh)\, U^n_{2jk}\,, \tag{13a}$$

$$P^n_{i2k} - P^n_{i0k} = (4/Reh)\, V^n_{i2k}\,, \tag{13b}$$

$$P^n_{N+1jk} - P^n_{N-1jk} = (4/Reh)\, U^n_{N-1jk}\,, \tag{13c}$$

$$P^n_{iN+1k} - P^n_{iN-1k} = (4/Reh)\, V^n_{iN-1k}\,. \tag{13d}$$

The periodic conditions (8) and (9) become

$$U^n_{ij1} = U^n_{ijN} \qquad V^n_{ij1} = V^n_{ijN} \qquad W^n_{ij1} = W^n_{ijN} \qquad 1 \leqslant i, j \leqslant N \tag{14}$$

and

$$P^n_{ij1} = P^n_{ijN}\,, \qquad 1 \leqslant i, j \leqslant N. \tag{15}$$

In Eq. (10), terms A and C are standard central differences to $\partial U/\partial t$ and $-\partial P/\partial x$, respectively. D is the Dufort–Frankel approximation for the diffusion terms. B is a new finite-difference approximation for the convective terms. It may be thought of as a central difference approximation for the average of the two ways of writing the convective terms given in Eqs. (1) and (4). This particular form of differencing for the convective term is important since it preserves the finite-difference analog of the energy conserving property of the convective terms in the continuous integral energy equations, i.e., the finite difference analog of

$$\int_0^1 \int_0^1 \int_0^1 U_i(U_j(\partial U_i/\partial x_j))\, dx\, dy\, dz = 0.$$

Arakawa [5] has presented several schemes which conserve energy in a two-dimensional stream function and vorticity formulation. The differencing scheme for the convective terms presented here is believed to be a new energy conserving scheme for three dimensional calculations. It should be mentioned that for finite time steps, the convective part of the differenced equations is no longer exactly energy conserving so that nonlinear computational instability may still develop at very high Reynolds numbers.

Conditions (13a–d) allow the pressure to fluctuate at the wall in accordance with the governing differenced version of the Navier–Stokes equations. Another condition on the pressure was also used, namely, pressure was not allowed to fluctuate on the walls. A comparison of results of tests in which first one and

then the other type of pressure boundary condition was used showed a similar kind of convergence with mesh refinement. However, for the mesh sizes used, the convergence of quantitites of interest as the mesh is refined is more clearly seen in the examples using the condition that allows no pressure fluctuation. The overall scheme may be shown to be an $0\{(\Delta t/h)^2 + h\}$ approximation to the differential system [4].

TABLE I

Tabulation of Computed Runs[a]

Run	N, Z	Δt	PF	I.C.	T	D	P.C.	hr
1	7, 7	standard	0.5	run 2	185	39	B	1.6 (1)
2	7, 7		2.0	prev. run	266	110		4.7 (1)
3	7. 7		3.5	run 5	214	113		5.3 (1)
4	7, 13		3.5	I.C. 1	78	43		3.5 (1)
5	7, 7		5.0	prev. run	148	91		4.4 (1)
6	7, 7		7.0	run 5	165	108		6.1 (1)
7	9, 9		0.7	run 8	111	33		3.3 (1)
8	9, 9		1.2	run 9	152	61		5.5 (1)
9	9, 9		3.0	run 10	105	63		6.2 (1)
10	9, 9		5.0	run 11	77	58		6.3 (1)
11	9, 9		7.0	I.C. 2	48	38		4.5 (1)
12	9, 9		12.0	run 11	49	52		7.0 (1)
13	9, 9		12.0	run 12	44	19	A	4.8 (1)
14	11, 11		0.79	run 16	34	28	B	5.5 (1)
15	11, 11		7.0	I.C. 3	37	33		7.5 (1)
16	11, 11		12.0	I.C. 3	47	43		13.2 (1)
17	11, 11		12.0	run 15	22	26		7.2 (1)
18	11, 11		12.0	run 17	24	14	A	6.3 (1)
19	17, 17		0.8	I.C. 4	32	12	B	3.0 (2)
20	17, 17		2.25	I.C. 5	33	17		4.1 (2)
21	17, 17	$\frac{1}{2}$ standard	2.25	I.C. 5	35	18		9.3 (3)
22	17, 17		5.0	I.C. 5	17	14		3.3 (2)
23	17, 17		12.0	I.C. 6	23	30		8.2 (2)
24	7, 7		0.7	I.C. 7	33	10		0.5 (1)

Table continued

TABLE I (*continued*)

[a] Explanation of column headings:

N, Z: Mesh points in (x, y) and z directions, respectively.

Δt: "Standard" corresponds to the linear stability criterion, $\Delta t \mid W \mid_{\max} \simeq 0.4h$.

PF: Relative pressure gradient; $PF = 1$ corresponds to a center line velocity of $W = 1.0$ if the flow is laminar.

I.C.: Initial Conditions; the designation "run" followed by a number means the example was started from the result of the designated run number. Other initial conditions were used for the other runs [4].

T: Dimensionless time, $T = \sum_{i=1}^{n} \Delta t_i$, where n is the total number of time steps taken.

D: Diameters traveled at mean axial velocity of the fluid, $D = \sum_{i=1}^{n} \Delta t_i \bar{W}_i$, where n is defined under T above.

P.C.: Pressure condition used: A corresponds to equation (13); B corresponds to no pressure fluctuation on walls.

hr: computer time used for each example; the numbers in parantheses designate the machine used. (1) UNIVAC 1107; (2) I.B.M. 360/75; (3) C.D.C. 6600. For this problem, the ratio of machine speeds is on the order of 1:4.26:4.02 for (1):(2):(3).

Note: Runs 3 and 4 have the same conditions except that run 4 has a test section approximately twice as long. The results of both runs plot as the same point on Fig. 6, confirming the assumption that a cubic test section is long enough.

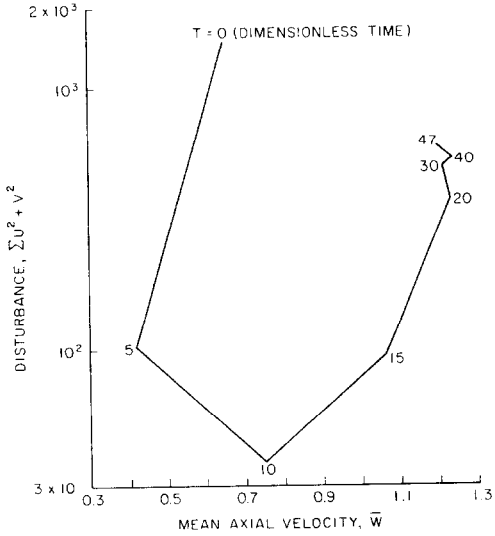

FIG. 3. Approach to sustained state.

4. Numerical Experiments

The numerical experiments are defined in Table I. A typical experiment is conducted by first assigning a Reynolds number, mean pressure gradient and an initial velocity field. The velocities are then stepped forward in time using Eq. (10) and the analogous equations for V and W. The elliptic equation for the pressure in terms of velocity is also solved at each time level. The numerical integration is continued forward in time until a sustained state is reached. It has been found that this sustained state can be characterized by plotting the energy of the secondary flow, $E_s = \sum_{ijk} (U_{ijk}^{n^2} + V_{ijk}^{n^2})$, versus the mean axial velocity, $\overline{W}^n$, with dimensionless time, $T = \sum_{i=1}^{n} \Delta t_i$, as a parameter. An example of this characterization is given in Fig. 3. It can be seen that after a long migration, the path eventually settles down into a small area. It is assumed that once E_s and W have reached these relatively stationary values that the velocity field is statistically steady so that meaningful averages of other quantities may be computed. The termination of each run is based on the use of plots like Fig. 3.

5. Qualitative Results

Two distinct types of solutions have been obtained from the finite-difference scheme. One type is characterized by a decay of the disturbance present in the initial condition to an insignificantly low level. The velocity approaches the analytical solution for laminar flow in square ducts [6].

As the axial pressure gradient is increased, another type of solution is obtained from the finite-difference scheme. For this type, the initial disturbance approaches a final steady value. The level of this steady value is significant in that it substantially changes the mean properties of the flow. The characteristics of this type of solution will be discussed in detail.

One of these characteristics of the computed flow is the independence of the sustained state from the initial conditions. Figure 4 shows the results of two runs employing the same set of parameters, but with different initial conditions. These are runs 16 and 17 of Table I. It can be seen that both examples settle down in the same area of the disturbance–mean velocity plane after starting from widely separated points. The estimated sustained state mean velocity (and hence the Reynolds number and friction factor) for both flows is virtually identical. This independence of the mean properties of the fully developed flow from the initial disturbance is, of course, a characteristic of real turbulent flows. From a practical standpoint, it can be seen that the choice of initial conditions may have a substantial influence on the length of simulated flow time, and hence computational time, required to reach the sustained state area.

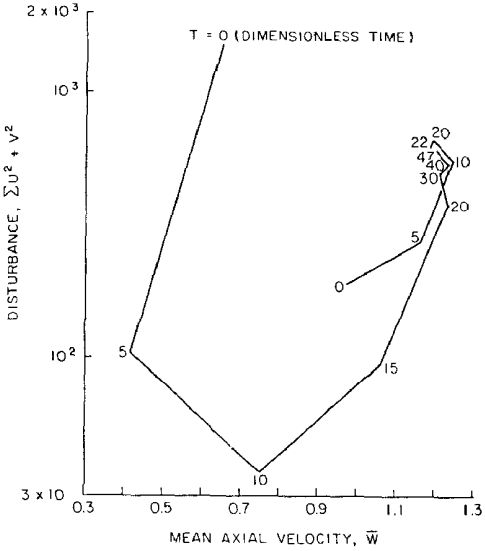

FIG. 4. Approach to sustained state from different initial conditions.

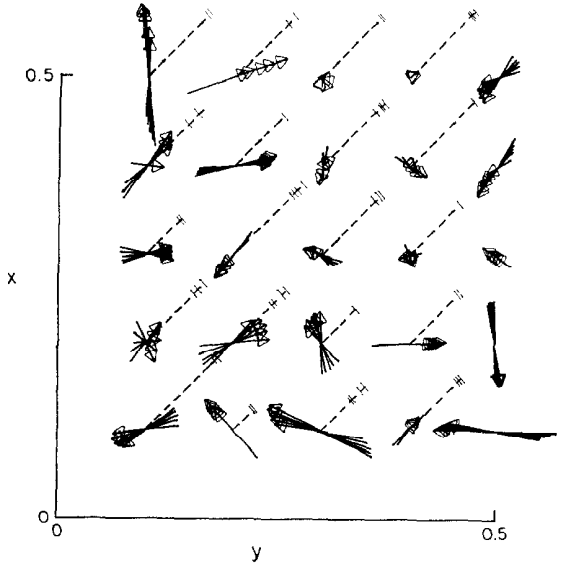

FIG. 5. Dynamic nature of sustained state.

Another qualitative characteristic of the computed flow that may be identified with turbulence is the dynamic nature of the sustained state. Figure 5 shows a representation of a portion of the velocity field for run 17 of Table I after the sustained state area has been reached. Some of the points on one mesh plane perpendicular to the axial direction are exhibited. The solid vectors are the secondary or cross plane velocities. They indicate direction and magnitude. The dotted lines represent downstream velocities perpendicular to the plane of the page. The downstream velocities are drawn to about one-third the scale of the secondary velocities. The five vectors at each mesh point represent a time sequence, with every second time step being represented. The total of nine time steps occurring from the first to the last field represents enough time to travel approximately one mesh interval at the mean axial velocity for this example.

6. Quantitative Results and Evidence of Convergence

Figure 6 displays the sustained state results of all the runs on a friction-factor Reynolds number correlation plot for round pipes. According to the measurements of Hoagland [7] and Hirose and Asand [8], the friction factors for square ducts are only about 5% lower than those for round pipes in the turbulent regime. The numbers next to the data points refer to run numbers from Table I.

It is obvious that, for the mesh sizes tested, the departure from the laminar line takes place at Reynolds numbers far below the experimentally determined value. The calculated transition Reynolds numbers are 250–550, depending on pressure gradient and mesh spacing. The collected data and analysis of Hanks and Ruo [9]

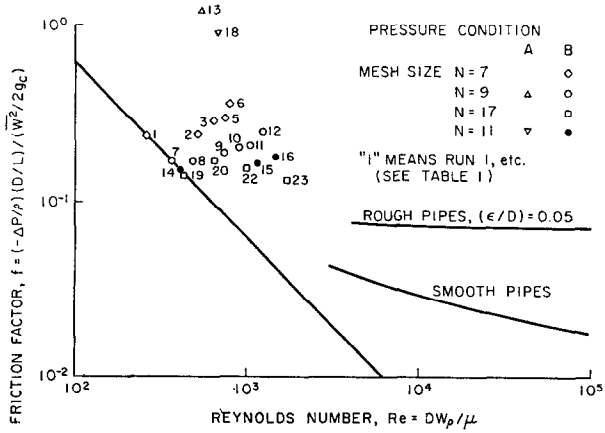

FIG. 6. Reynolds Number–Friction Factor Correlation.

indicate that the critical Reynolds number for square duct flow is almost identical to that for a round pipe, i.e., $Re_c \simeq 2050$. The examples indicate that this early departure is not a function of the initial disturbance, but is rather a result of the relatively coarse mesh spacings used. It can be seen in Fig. 6 that the critical Reynolds number increases as the mesh becomes finer.

The computed points at each mesh size in Fig. 6 show a tendency toward reduction of friction factor with increasing Reynolds number after initial departure from the laminar line, as would be expected. However, as the Reynolds number increases further, the points begin to rise. This anomalous behavior results from the difference approximations and is related to the inability of the grid to represent the steep velocity gradients that arise near the wall. This deficiency of the difference scheme can be demonstrated by deriving the integral axial momentum equation associated with the difference equation in a manner analogous to its derivation in the continuous form. This derivation and an analysis of the resulting equation is given in Appendix 1. Other such integral equations associated with the difference scheme can be derived and used to analyze the results obtained from the computations [4].

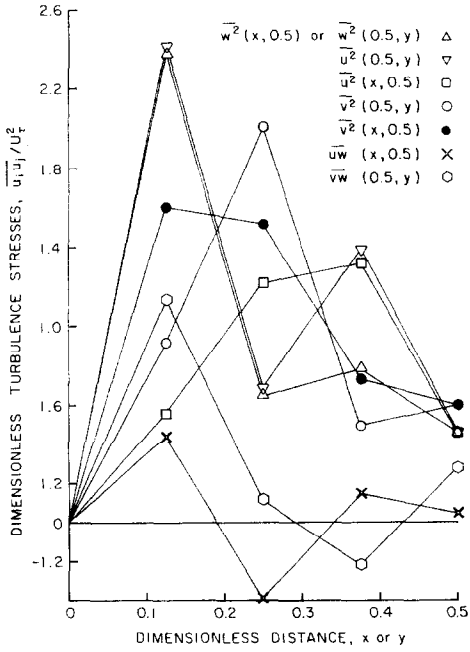

FIG. 7. Reynolds stresses.

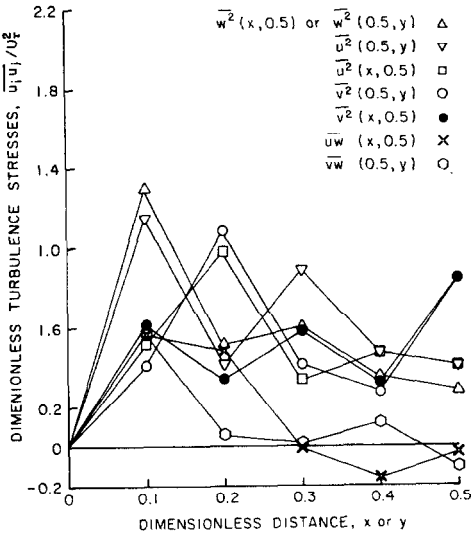

FIG. 8. Reynolds stresses.

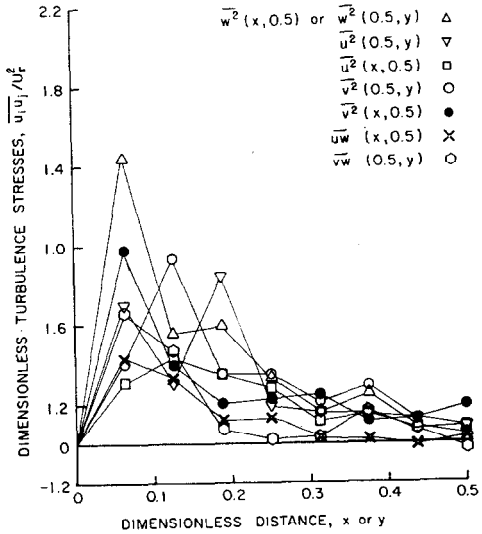

FIG. 9. Reynolds stresses.

It can be seen in Fig. 6 that the runs made at the finest mesh, $N = 17$, have a qualitatively different behavior than those made at the coarser meshes when displayed on the Reynolds number-friction factor plot. They suggest a curve that much more closely resembles the experimentally derived curve in the transition

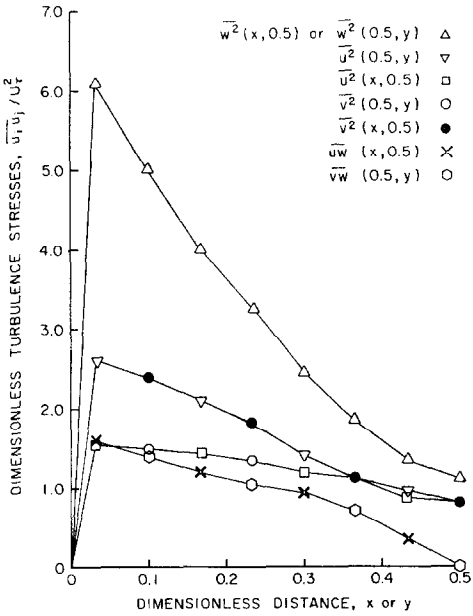

FIG. 10. Reynolds stresses from data of Brundrett and Baines, Re = 83,000.

region of real turbulent flows. In particular, the demarcation between "laminar" and "turbulent" flow becomes sharper.

Further effects of reducing the mesh size may be seen by comparing the Reynolds stresses computed from runs 12, 16, and 23 of Fig. 6. All parameters except mesh size are identical for each of these runs. The mean pressure gradient assigned would correspond to a Reynolds number of about 7 000, based on duct width, if the flow were laminar. Thus, the computed solutions should be converging to a turbulent flow in the transition region as the mesh is refined. It is difficult to know what should characterize the Reynolds stresses in this region. Nevertheless, some comparisons will be made that seem to indicate convergence to a quantitative description of what might be expected in real flows in the transition region.

Figures 7, 8 and 9 are Reynolds stress profiles averaged in the z direction at one time level for runs 12, 16 and 23, respectively. They are computed from the fluctuating part of the velocity defined as the deviation of the total velocity at a point from the z averaged velocity at one time level. For comparison Fig. 10 shows the data of Brundrett and Baines [10] taken in a square duct at a Reynolds number of 83 000. The Reynolds stresses in each case have been nondimensionalized by the friction velocity W_τ, defined as

$$W_\tau = \sqrt{\overline{-\nu \frac{d\overline{W}}{dx}\Big|}} \qquad \text{averaged at wall.}$$

For the computed examples, W_τ is based on the mean pressure gradient. There is some qualitative agreement between the computed Reynolds stress profiles and the experimentally measured ones. In general, the largest values of the stresses occur near the wall. This is more in evidence as the mesh is refined. There is a tendency for the axial energy component $\overline{w'^2}$ to assume the largest value of all the stresses. Again, this is more evident as the mesh is refined. Furthermore, the stresses $\overline{u'w'}$ and $\overline{v'w'}$ tend to be smaller than the others, and to approach zero at the center. The anomalous negative values of $\overline{u'w'}$ and $\overline{v'w'}$ occurring at meshes $N = 9$ and $N = 11$ are almost absent for $N = 17$. The intensity of the Reynolds stresses can be seen to decrease with increasing N for the three runs. The intensity of the Reynolds stresses in all three runs is substantially less than that for the experimental data. However, since the data were obtained at a much higher Reynolds number, this is to be expected. It should be pointed out that there is some variation in the profiles depending on what time level is chosen. Furthermore, substantial improvement may be obtained in averaged quantities by averaging over a number of time levels as well as in the z direction. This may be seenby comparing Fig. 11, which is a time and space average of run 16, with Fig. 8, which is only a space average of the same run. The length of time averaging permitted approximately five diameters to be traveled at the mean velocity.

In summary of this part, examination of the results of runs at various mesh sizes indicates that qualitative and quantitative improvement in the description of turbulent flows is being achieved as the mesh is refined.

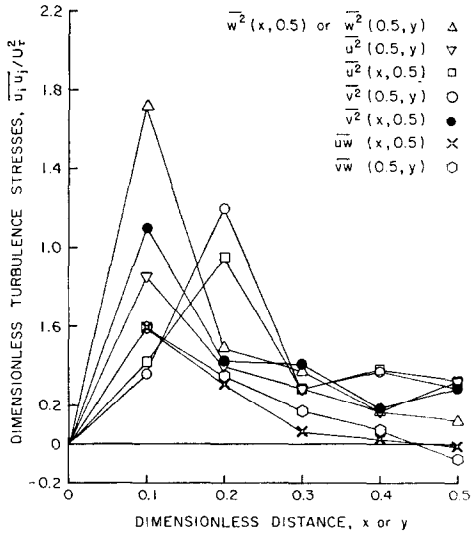

FIG. 11. Reynolds stresses, time and space average.

7. Estimate of Computing Requirements for Quantitative Results

The results of the computations have been used to estimate computing requirements to achieve quantitative results at various Reynolds numbers. The method of estimation assumes (1) the scheme is of $O(h)$, (2) the number of iterations needed to relax the pressure equation increases linearly with the number of mesh points required to give quantitative results, (3) the fluid must travel one entry length to become fully developed, and (4) the required mesh size decreases in proportion to the dissipation scale as the Reynolds number increases. The details of this development appear in Ref. [4].

Computing times on the various machines that were tried for some representative Reynolds numbers based on this estimate are given in Table II. It can be seen that only at Re = 4000 are the computing times on the fastest two machines even marginally practicable.

TABLE II

Estimate of Computing Requirements (in hours)

	Reynolds numbers			
Computer	4×10^3	10^4	5×10^4	10^5
Univac 1107	171	3.4×10^3	6.8×10^5	6.8×10^6
CDC 6600	43	8.5×10^2	1.7×10^5	1.7×10^6
IBM 360/75	40	8.0×10^2	1.6×10^5	1.6×10^6

8. Conclusions

A new stable, consistent, finite-difference approximation to the Navier–Stokes equations has been developed. It contains no predisposition toward turbulence, such as a built-in turbulence theory to represent effects of submesh size motions.

Extensive numerical testing of the finite-difference scheme has been performed. At low Reynolds numbers laminar solutions are obtained. At higher Reynolds numbers, analysis and comparison of results for the sustained flow solutions at successively finer meshes give strong indication that the solutions are converging to a quantitative description of turbulent flows. However, the results show that a low order approximation finite-difference scheme employing no representation for effects of sub-mesh size motions, such as the scheme used in this work, would require excessive computing time in order to obtain quantitative results.

APPENDIX I: Derivation and Analysis of the Integral Axial Momentum Equation Associated with the Finite Difference Scheme

The finite-difference analog of the integral axial momentum equation will be derived here from the finite-difference version of the axial momentum equation. Observations on its usefulness for interpreting the results of numerical computations will then be made.

For brevity, the derivation will be done in only two space dimensions. By way of analogy, we have for the continuous case.

$$\int_0^1 \int_0^1 \left\{ \frac{\partial W}{\partial t} + \frac{1}{2}\left(U \frac{\partial W}{\partial x} + W \frac{\partial W}{\partial z} \right) + \frac{1}{2}\left(\frac{\partial (UW)}{\partial x} + \frac{\partial (W^2)}{\partial z} \right) \right.$$
$$\left. = -\frac{\partial P}{\partial z} - \frac{\partial \bar{P}}{\partial z} + \frac{1}{\mathrm{Re}}\left(\frac{\partial^2 W}{\partial x^2} + \frac{\partial^2 W}{\partial z^2} \right) \right\} dx\, dz.$$

Carrying out the integration and making use of the periodic condition on velocity and pressure in the z direction yields

$$\overbrace{\int_0^1 \int_0^1 \frac{\partial W}{\partial t}\, dx\, dz}^{\mathrm{A}} = \overbrace{-\int_0^1 \Delta \bar{P}\, dx}^{\mathrm{B}} + \overbrace{\frac{1}{\mathrm{Re}} \int_0^1 \left[\frac{\partial W(1, z)}{\partial x} - \frac{\partial W(0, z)}{\partial x} \right] dz}^{\mathrm{C}}. \tag{A1}$$

In (A1), A represents the rate of change of axial momentum. B is the net pressure force acting on the fluid in the periodic section, and C is the net drag due to viscous shear at the wall.

In the finite-difference case, summations replace integrals. Thus we wish to evaluate

$$\sum_{i=2}^{N-1} \sum_{k=1}^{N-1} \left[\frac{W_{ik}^{n+1} - W_{ik}^{n-1}}{2\Delta t} + \frac{1}{2}\left(U_{ik}^n \frac{W_{i+1k}^n - W_{i-1k}^n}{2h} + W_{ik}^n \frac{W_{ik+1}^n - W_{ik-1}^n}{2h} \right) \right.$$
$$+ \frac{1}{2}\left(\frac{U_{i+1k}^n W_{i+1k}^n - U_{i-1k}^n W_{i-1k}^n}{2h} + \frac{W_{ik+1}^{n^2} - W_{ik-1}^{n^2}}{2h} \right)$$
$$= -\frac{P_{ik+1}^n - P_{ik-1}^n}{2h} - \frac{d\bar{P}}{dz}$$
$$\left. + \frac{1}{\mathrm{Re}}\left(\frac{W_{i+1k}^n + W_{i-1k}^n + W_{ik+1}^n + W_{ik-1}^n - 2(W_{ik}^{n+1} + W_{ik}^{n-1})}{h^2} \right) \right] h^2. \tag{A2}$$

The time derivative term from (A2) is simply summed and becomes

$$\sum_{i=2}^{N-1}\sum_{k=1}^{N-1}\frac{W_{ik}^{n+1}-W_{ik}^{n-1}}{2\Delta t}h^2. \tag{A3a}$$

The approximation to the first form of writing the convective terms is treated as follows:

$$\frac{1}{2}\left[\frac{1}{2h}\sum_{i=2}^{N-1}\sum_{k=1}^{N-1}U_{ik}^{n}(W_{i+1k}^{n}-W_{i-1k}^{n})\right]h^2$$

$$=\frac{1}{2}\left[\frac{1}{2h}\sum_{i=2}^{N-1}\sum_{k=1}^{N-1}W_{ik}^{n}(U_{i-1k}^{n}-U_{i+1k}^{n})\,h^2\right], \tag{A3b}$$

where the no slip condition at the wall has been used to obtain expression (A3b). Similarly, using the periodic condition in k, we obtain

$$\frac{1}{2}\left[\frac{1}{2h}\sum_{i=2}^{N-1}\sum_{k=1}^{N-1}W_{ik}^{n}(W_{ik+1}^{n}-W_{ik-1}^{n})\right]h^2$$

$$=\frac{1}{2}\left[\frac{1}{2h}\sum_{i=2}^{N-1}\sum_{k=1}^{N-1}W_{ik}^{n}(W_{ik-1}^{n}-W_{ik+1}^{n})\right]h^2. \tag{A3c}$$

The approximation to the second form of writing the convective terms is treated as follows:

$$\frac{1}{2}\left[\frac{1}{2h}\sum_{i=2}^{N-1}\sum_{k=1}^{N-1}(U_{i+1k}^{n}W_{i+1k}^{n}-U_{i-1k}^{n}W_{i-1k}^{n})\right]h^2$$

$$=\frac{1}{2}\left[\frac{1}{2h}\sum_{k=1}^{N-1}(U_{N-1k}^{n}W_{N-1k}^{n}-U_{2k}^{n}W_{2k}^{n})\right]h^2, \tag{A3d}$$

using the no slip wall condition and the telescoping nature of the summation.

However, because of the periodic condition in k, we have

$$\frac{1}{2}\left[\frac{1}{2h}\sum_{i=2}^{N-1}\sum_{k=1}^{N-1}(W_{ik+1}^{n^2}-W_{ik-1}^{n^2})\right]h^2=0$$

The pressure terms, when summed, become

$$-\frac{1}{2h}\sum_{i=2}^{N-1}\sum_{k=1}^{N-1}\left(P_{ik+1}^{n}-P_{ik-1}^{n}+2h\frac{d\bar{P}}{dz}\right)h^2$$

$$=\frac{1}{2h}\sum_{i=2}^{N-1}2h(N-1)\frac{d\bar{P}}{dz}h^2$$

$$=\sum_{i=2}^{N-1}\frac{d\bar{P}}{dz}h, \tag{A3e}$$

since the P's cancel because of the telescoping sum and the periodic boundary condition, and use has been made of the relation $h=1/(N-1)$.

The viscous terms are treated as follows:

$$\frac{1}{Reh^2}\sum_{i=2}^{N-1}\sum_{k=1}^{N-1}(W_{i+1k}^{n}+W_{i-1k}^{n}-2W_{ik}^{*})h^2$$

$$=\frac{2}{Reh^2}\sum_{i=2}^{N-1}\sum_{k=1}^{N-1}(W_{ik}^{n}-W_{ik}^{*})h^2-\frac{1}{Reh}\sum_{k=1}^{N-1}(W_{2k}^{n}+W_{N-1k}^{n})h, \tag{A3f}$$

where $W_{ik}^{*}\equiv\frac{1}{2}(W_{ik}^{n+1}+W_{ik}^{n-1})$. Similarly,

$$\frac{1}{Reh^2}\sum_{i=2}^{N-1}\sum_{k=1}^{N-1}(W_{ik+1}^{n}+W_{ik-1}^{n}-2W_{ik}^{*})h^2$$

$$=\frac{2}{Reh^2}\sum_{i=2}^{N-1}\sum_{k=1}^{N-1}(W_{ik}^{n}-W_{ik}^{*})h^2, \tag{A3g}$$

where there is no second term in (A3g) because of the periodic condition.

Combining (A3a–g), we now have the finite-difference approximation to the

integral momentum equation in a form which can be compared with (A1). Thus,

$$\overbrace{\sum_{i=2}^{N-1}\sum_{k=1}^{N-1}\frac{(W_{ik}^{n+1}-W_{ik}^{n-1})}{2\Delta t}h^2}^{A'}$$

$$=\overbrace{-\sum_{i=2}^{N-1}\frac{d\bar{P}}{dz}h}^{B'}$$

$$\overbrace{-\frac{1}{Re}\sum_{k=1}^{N-1}\frac{(W_{2k}^{n}+W_{N-1k}^{n})}{h}h}^{C'}$$

$$\overbrace{-\frac{1}{2}\sum_{i=2}^{N-1}\sum_{k=1}^{N-1}W_{ik}^{n}\left(\frac{U_{i-1k}^{n}-U_{i+1k}^{n}}{2h}+\frac{W_{ik-1}^{n}-W_{ik+1}^{n}}{2h}\right)h^2}^{E1}$$

$$\overbrace{-\frac{1}{4}\sum_{k=1}^{N-1}(U_{N-1k}^{n}W_{N-1k}^{n}-U_{2k}^{n}W_{2k}^{n})h^2}^{E2}$$

$$\overbrace{+\frac{4}{\mathrm{Re}}\sum_{i=2}^{N-1}\sum_{k=1}^{N-1}\frac{(W_{ik}^{n}-W_{ik}^{*})}{h^2}h^2}^{E3}. \tag{A4}$$

It can be seen that the terms to be summed in A′, B′ and C′ are consistent approximations to the integrands of A, B and C, respectively. However, E1, E2, and E3, which can be shown to be of order $O(h^2)$, $O(h^2)$ and $O[(\Delta t/h)^2]$, respectively, may be thought of as spurious momentum generators or drag terms since they go to zero as h and Δt go to zero, but otherwise have a finite value. During the computations, evaluation of the terms in (A4) showed that E1 and E3 remained insignificant. However, as the mean axial pressure gradient was increased, E2 assumed larger and larger negative values. Since E2 involves the product of velocities one mesh point inside the wall, which with a fine enough mesh should be very small, the nature of the error from E2 is a mesh size that is inadequate to represent the boundary layer properly. The effect of this spurious drag from E2 as seen on the Re-f plot (Fig. 6) is the erroneous rapid increase of f as the Reynolds number gets larger.

ACKNOWLEDGMENTS

The research was supported by the National Science Foundation, Grant GK 778 and Case Western Reserve University. Computations were performed at the Andrew R. Jennings Computing Center of Case Western Reserve University, the Gulf Research and Development Company in Pittsburgh, PA. and the National Center for Atmospheric Research, Boulder, CO. The computer time and staff contributions given by each of these organizations is sincerely appreciated.

REFERENCES

1. S. ORSZAG, *Phys. Fluids Suppl. 2* **12** (1969), 251.
2. J. W. DEARDORFF, *J. Fluid Mech.* **41** (1970), 453.
3. S. CORRSIN, *Amer. Sci.* **49** (1961), 300.
4. F. M. GALLOWAY, JR., On a finite-difference approach to turbulence problems, Ph.D. Thesis, Case Western Reserve University, 1968.
5. A. ARAKAWA, *J. Comput. Phys.* **1** (1966), 119.
6. R. J. CORNISH, *Proc. Royal Soc. A* **120** (1928), 691.
7. L. C. HOAGLAND, Ph.D. thesis, Massachusetts Institute of Technology, 1960.
8. K. HIROSE AND Y. ASANO, *Mem. School Eng. Okayama Univ.* **4** (1969), 13.
9. R. W. HANKS AND H. C. RUO, *I & EC Fundamentals* **5** (1966), 559.
10. E. BRUNDRETT AND W. BAINES, *J. Fluid Mech.* **19** (1964), 375.